CFD Simulation on the Optimum Pulse Tube Volume for a 120Hz Pulse Tube Cryocooler

Y. Yuan[1], X. Zhi[1], W. He[1], Z. Gan [1,2], L. Qiu [1]

[1]Institute of Refrigeration and Cryogenics, Zhejiang University
Hangzhou, 310027, P.R. China
[2]Shanghai Institute of Technical Physics, CAS, 200083, P. R. China

ABSTRACT

The expansion efficiency of a pulse tube is significantly influenced by its dimensions, and its associated losses can be minimized by choosing an appropriate volume. In such a case the expansion efficiency increases, as well as the overall efficiency. This paper calculates the expansion efficiency of various pulse tubes with different volumes using a CFD simulation. The results of the simulation play an important role in guiding the design of pulse tubes operating at very high frequencies.

INTRODUCTION

Application in the aerospace field, such as the cooling of infrared detectors and optic devices, has strict requirements on mass, volume, and fast cool-down of cryocoolers. As pulse tube coolers have intrinsic advantage of high reliability, low vibration and simple structure, they are desirable in aerospace application. Study on pulse tube coolers operating in the hundred Hz range has developed rapidly in recent years. And how to raise operating frequency to increase power density so that overall mass and volume could reduce while maintain the same efficiency or cooling power is becoming currently heated research topic.

In 2005 Radebaugh of the National Institute of Standards and Technology first pointed out that power density could greatly increase if the operating frequency increases according to his analysis[1]. However, higher charging pressure and smaller volume should also be adopted to maintain high efficiency. This theory indicates the right direction for the miniaturization of coolers with a large cooling power. Afterwards in 2006 NIST designed an in-line pulse tube cooler operating at 120Hz and got 3.35W cooling power at 80K which verified their theory and ignited the interest in research into pulse tube coolers operating in the hundred Hz range[2]. In the same year, the Chinese Academy of Science designed the first 300Hz in-line thermo-acoustically driven pulse tube cooler and got a no load temperature below 100K[3]. This machine was improved in 2009 and obtained a no load temperature of 68K and 1.16W cooling power at 80K with a charge pressure of 4.1 MPa and an input power of 1 KW[4]. In 2008 NIST also designed a 150Hz in-line pulse tube cooler whose regenerator is only 27mm long and has an inner diameter of 4.4 mm, while it could obtain a no load temperature of 97.5K due to limited phase shift ability in the inertance tube[5]. Nonetheless, it took only 100 seconds to cool down from room

Cryocoolers 17, edited by S.D. Miller and R.G. Ross, Jr.

temperature to 100K, which significantly reduced cooling down time. In the same year, Northrop Grumman Space Technology designed a very attractive single-stage coaxial pulse tube cooler which weighed only 857g and produced 1.3W cooling power at 77K[6]. In 2009, Zhejiang University designed a 120Hz in-line pulse tube cooler which produced a no load temperature of 49.6K and 8W cooling power at 78.5K[7]. In 2010, the Chinese Academy of Science designed a 100Hz in-line pulse tube cooler which got a no load temperature of 31.8K and 12.4W cooling power at 77K with an input power of 180W, and the overall Carnot efficiency was up to 18.94%[8]. In the same year, the Chinese Academy of Science also designed a 300Hz two-stage thermo-acoustically driven pulse tube cooler whose first stage was a coaxial-type and the second stage was an in-line type[9]. The cold head of the second stage gained a no load temperature of 57.9K and 0.5W cooling power at 81.88K with a charge pressure of 3.8 MPa and an input PV power of 1.5KW. In 2011, France CEAEA designed a 100Hz in-line pulse tube cooler which obtained a no load temperature of 79.8K, 0.98W cooling power at 120K with an input PV power of 20W and 0.22W cooling power at 77K with an input PV power of 30W[10].

The pulse tube is a key component of a pulse tube cryocooler, whose expansion efficiency strongly influences the overall efficiency. Various losses in the pulse tube, including the wall and gas conduction loss, the pumping loss, the shuttle loss, the DC-flow loss, the gas mixing loss and frictional resistance loss, influence expansion efficiency, yet some losses can be minimized by choosing an appropriate volume. In this report[11-12], researchers have achieved favorable performance by making use of larger pulse tube volumes. In 2011, Zhejiang University built a two-dimension non-adiabatic model for pulse tube in the 80-300K temperature region utilizing CFD method and studied optimum pulse tube volume matching a constant cold end expansion volume[13].This study found that the optimum pulse tube volume should be 13 times the cold end expansion volume rather than 3-5 times given by traditional adiabatic models, and the existence of non-adiabatic loss between tube wall and gas results in a larger pulse tube volume which should be adopted to obtain a comparatively high efficiency. The study also analyzed the intrinsic relationship between the pulse tube volume and the heat losses. Nevertheless, as that research is simply for traditional Stirling pulse tube cooler (40Hz), this paper also makes use of that two-dimensional non-adiabatic model to calculate the optimum pulse tube volume for a 120Hz pulse tube cryocooler.

CFD MODEL OF PULSE TUBE

Physical Model

Parameters in the model built in this paper is from an established single-stage U-type pulse tube cryocooler, which includes a cold end heat exchanger, a pulse tube and a hot end heat exchanger, as shown in Figure 1. The adiabatic model assumes the wall has no thickness, while in the non-adiabatic model both the pulse tube and the heat exchanger wall have the thickness of 0.35 mm. The cold and hot end heat exchanger is filled with 80 mesh copper screens. The relationship between the pulse tube volume Vpt and the cold end expansion volume Vexp is shown as below:

$$V_{pt}/V_{exp}=n \quad (n=3、5、7、9、11、13、15) \tag{1}$$

Where the cold end expansion volume Vexp means the total gas volume flowing into or out of the pulse tube cold end in one direction is a constant here: 1.4332×10-6 m3. In all pulse tubes, the ratio of length to diameter is set to 5.078, other parameters are shown in Table 1 and 2.

The grid model of the pulse tube is shown in Figure 1(b), and all the components adopt a rectangle grid. In order to describe the fluid characteristic of the boundary layer more accurately, the grid near the tube wall is made denser. The total number of the grid is between 4536-7704.

In the 80-300K temperature region, working helium is treated as an ideal gas. The charging pressure is 3.5 MPa and operating frequency is 120 Hz. The pressure ratio at the cold end is 1.2, the inlet boundary condition is the mass flow at 80K and the outlet boundary condition is pressure at 300K. In the CFD model, both the inlet and outlet boundary condition are defined by user-defined functions written in the C programming language, their formulas are as below:

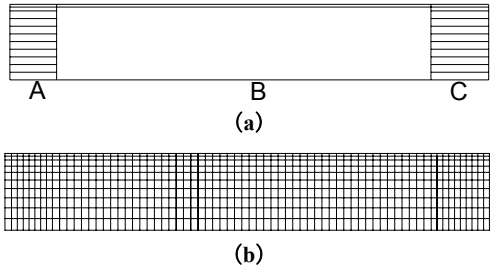

Figure 1. Schematic diagram of pulse tube structure

Table 1. Parameters of pulse tube model

Symbol	Diameter (mm)	Length (mm)	Wall thickness (mm)	Porosity
Section A：cold end heat exchanger	Dpt	6.5	0/0.35	0.78
Section B：pulse tube	Dpt	Lpt	0/0.35	1
Section C：hot end heat exchanger	Dpt	8	0/0.35	0.78

Table 2. Parameters of pulse tube (The ratio of length to diameter Lpt /Dpt=5.078)

n	3	5	7	9	10	11	12	13	14	15
Vpt(cm^3)	4.30	7.17	10.03	12.90	14.33	15.77	17.20	18.63	20.06	21.50
Dpt (mm)	10.25	12.16	13.60	14.79	15.32	15.81	16.28	16.72	17.14	17.53
Lpt (mm)	52.07	61.73	69.06	75.10	77.78	80.29	82.65	84.89	87.01	89.04

$$\dot{m}_{in} = m_{amp} \cdot \sin(2\pi ft + \varphi) \tag{2}$$

$$p_{out} = p_0 + p_m \cdot \sin(2\pi ft) \tag{3}$$

Where p_m is the periodic pressure amplitude, f the is operating frequency, m_{amp} is the periodic mass flow amplitude, φ is the phase difference between the inlet mass flow and the outlet pressure, and all are constant for all models. The cold end and the hot end heat exchanger are adopted from a porous media model and are assumed to be of constant temperature, 80K and 300K respectively. All heat exchanger walls are set to an isothermal boundary and the outer wall of the pulse tube is an adiabatic boundary.

Fundamental control equation

The fluid regions in the model are a non-porous media region. The screen region is a porous media region. Continuity equation, momentum equation and energy equation are shown below[14-15]:

$$\frac{\partial}{\partial t}(\phi\rho_{\mathrm{f}}) + \nabla\left(\phi\rho_{\mathrm{f}}\vec{u}\right) = 0 \tag{4}$$

$$\frac{\partial}{\partial t}\left(\phi\rho_{\mathrm{f}}\vec{u}\right) + \nabla\left(\phi\rho_{\mathrm{f}}\vec{u}\vec{u}\right) = -\phi\nabla p + \nabla\cdot\left(\phi\tau\vec{u}\right) + S_{x(y)} \tag{5}$$

$$\frac{\partial}{\partial t}\left(\phi\rho_{\mathrm{f}}E_{\mathrm{f}} + (1-\phi)\rho_{\mathrm{s}}E_{\mathrm{s}}\right) + \nabla\cdot\left(\vec{u}\left(\rho_{\mathrm{f}}E_{\mathrm{f}} + p\right)\right) = \nabla\cdot\left[(\phi k_{\mathrm{f}} + (1-\phi)k_{\mathrm{s}})\nabla T + \left(\phi\tau\cdot\vec{u}\right)\right] \tag{6}$$

Where ϕ is porosity of porous media, S_x , S_y represents axial and radial momentum loss caused by resistance loss respectively, D_h is hydraulic diameter of mesh screens, k_{f} , k_{s} represents

conductivity coefficient of gas and solid respectively. For non-porous media region, $\phi = 1$, $S_{x(y)} = 0$. While for porous media region, the formula of resistance source term is shown as below:

$$S_{x(y)} = -\frac{1}{2D_h} C \rho_f \left|\vec{u}\right| \vec{u} \tag{7}$$

Where C is resistance coefficient of mesh screens. As there is not much research about radial resistance characteristic of mesh screens, mesh screens are assumed to bear the same characteristic in all directions. Both axial and radial resistance coefficient adopt the experimental formula recommended by thesis 16: $C = 129 / Re + 2.91 Re^{-0.103}$

This paper chooses standard k-ε turbulent model which is suitable for a comparatively large Reynolds number range, making use of the finite volume method and implicit formulation to discretize the control equations, adopting the PISO methodin solver which is pressure-velocity coupling, and the discretization scheme is a second order upwind scheme for convective term and central differencing scheme for diffusive term. By monitoring the periodic temperature and enthalpy flow at the pulse tube cold end to decide whether the calculation is steady or not, and the calculation is steady when the monitored parameters do not change any more. There are 200 time steps in one period and all models reach a steady-state after 100 periods.

Post-Processing of Parameters

The expansion efficiency of the pulse tube is defined by the ratio of enthalpy at the cold end to the PV power at the cold end, which also means the ability of transforming PV power to enthalpy; the definition formula is shown below:

$$\varepsilon_{pt} = \frac{\langle \dot{H} \rangle_c}{\langle \dot{pV} \rangle_c} = \frac{\langle \dot{pV} \rangle_c - T_c \langle \dot{S} \rangle_c}{\langle \dot{pV} \rangle_c} \tag{8}$$

The less the irreversible entropy generation caused by various losses in the expansion process, the more the enthalpy and cooling power is obtained. Based on the calculation results of the CFD model, the PV power and enthalpy in one period is obtained through the formulas below:

$$\langle \dot{pV} \rangle = \frac{1}{\tau} \int_0^{\tau} p dv = \frac{1}{n} \sum_{i=1}^{n} p_i v_i \tag{9}$$

$$\langle \dot{H} \rangle = \frac{1}{\tau} \int_0^{\tau} \dot{m} h dt = \frac{1}{n} \sum_{i=1}^{n} m_i h_i \tag{10}$$

Where n is the number of iteration steps in one period, p_i, v_i, m_i, h_i represents pressure, volume flow, mass flow and specific enthalpy in the time step of i respectively.

RESULTS AND ANALYSIS

Expansion Efficiency of Pulse Tube

The expansion efficiency of different pulse tubes is shown in Figure 2. For the adiabatic model, when the pulse tube volume is 5-7 times the cold end expansion volume, the gas piston in it already has the desirable ability for axially thermal insulation and gas flow insulation. The corresponding expansion efficiency is 87.7%-88.3%. When pulse tube volume is more than 13 times the cold end expansion volume, the expansion efficiency decreases due to flow resistance loss.

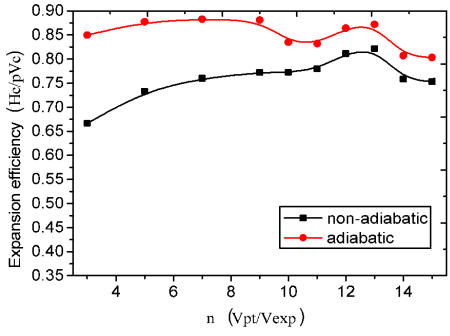

Figure 2. Expansion efficiency of varied pulse tube volumes

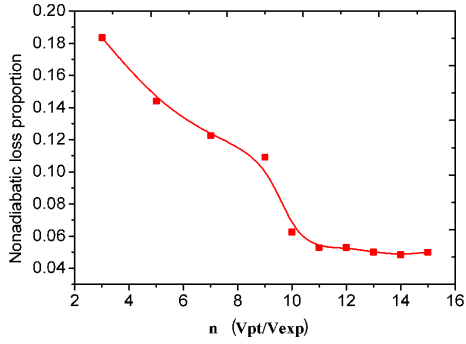

Figure 3. Non-adiabatic loss proportion of varied pulse tube volumes

For the non-adiabatic model, the pulse tube volume should be 13 times the cold end expansion volume so that the gas piston in it could have the desirable ability for axial thermal insulation and gas flow insulation. The corresponding expansion efficiency is 82.2%. The result differs from the adiabatic model. Figure 3 shows the non-adiabatic loss of different pulse tube volumes in the non-adiabatic model. It can be found that the non-adiabatic loss greatly influences the expansion efficiency at 3-11 times the cold end expansion volume. When the pulse tube volume is greater than 13 times the cold end expansion volume, the non-adiabatic loss nearly remains the same and increasing the pulse tube volume provides no improvement. Therefore, the real pulse tube operating in the hundred Hz range also need to utilize a larger volume than the optimum volume demonstrated by the adiabatic model so that the associated non-adiabatic loss is comparatively small and increases the expansion efficiency.

Gas Temperature Distribution Characteristic in Pulse Tube

Ideally, there is no viscous loss in the pulse tube so that the flow which remains laminar and temperature is uniform on the same cross-section. However, the boundary layer near the pulse tube wall causes that an uneven temperature in the same cross-section. Dot a, b, c, d in Figure 4 respectively represents four different state of inlet pressure at the pulse tube cold end. Figure 5 shows temperature distribution at state a and c (which respectively represents the compression and the expansion process). The isothermal line near the wall is curved. The reason is that the gas velocity in the boundary layer is different from that in tube center and there is a velocity gradient, so that the temperature is uneven in same cross-section. And the inhomogeneous temperature on the same cross-section could worsen the irreversible heat exchanging loss among gas in the tube.

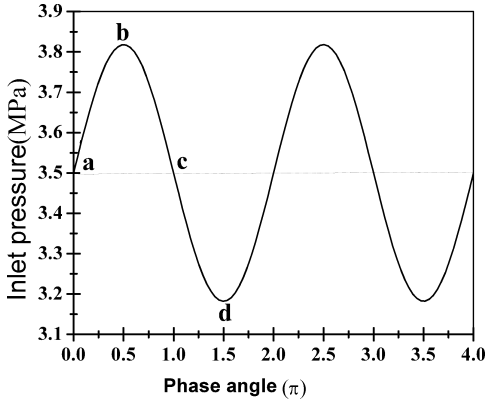

Figure 4. Inlet pressure at the pulse tube cold end

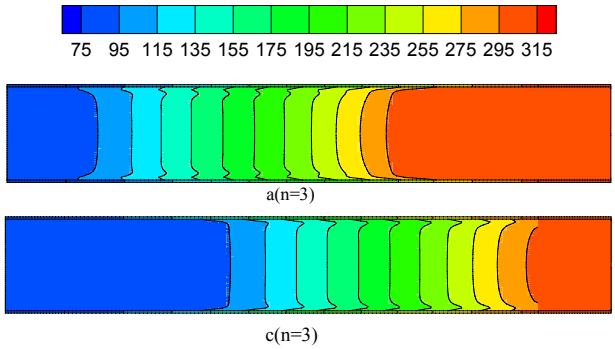

Figure 5. Temperature distribution at state a and c

Thesis 11 figures that the boundary layer near the pulse tube wall is found to be analogous between the gas piston and the tube wall. It is also pointed out that the temperature difference between moving gas and tube wall causes shuttle loss. For a constant cold end expansion volume, the displacement of gas piston in a smaller pulse tube is larger and the temperature gradient in a shorter pulse tube is more remarkable, both of which can result in more significant temperature difference between gas near wall and the tube wall when the gas piston is moving and between the gas in the boundary layer and main gas stream in the tube, which then generate more pumping loss and shuttle loss. It is the same case in the pulse tube operating in the hundred Hz range.

Figure 6 shows the temperature distribution near wall and on the wall of different pulse tube volumes in non-adiabatic model at state a and c. The gas temperature near the wall is higher than the wall temperature in the compression process and lower in the expansion process. The surface heat pumping presents a shuttle loss. For a pulse tube of 3 times the cold end expansion volume, the temperature difference between the gas near the wall and the tube wall is 19.32 K, 19.42 K respectively in the compression and the expansion process, which is far greater than that for pulse tube of 13 times the cold end expansion volume (5.4K, 5.11K), thus a pulse tube of 3 times the cold end expansion volume bears a larger shuttle loss. Figure 7 shows a temperature distribution near wall and on the axis of different pulse tube volumes in non-adiabatic model at state a and c. For pulse tube of 3 times of cold end expansion volume, temperature difference between gas near wall and axis is 15.63 K, 11.21 K respectively in compression and expansion process, which is more remarkable than that for pulse tube of 13 times the cold end expansion volume (10.55K, 9.07 K), thus pulse tube of 3 times the cold end expansion volume assumes greater pumping loss. Therefore, larger temperature difference between gas near wall and wall and worse gas temperature homogeneity on the same cross-section is the intrinsic reason why the pulse tube of 3 times the cold end expansion volume bears a higher heat loss than pulse tube of 13 times the cold end expansion volume.

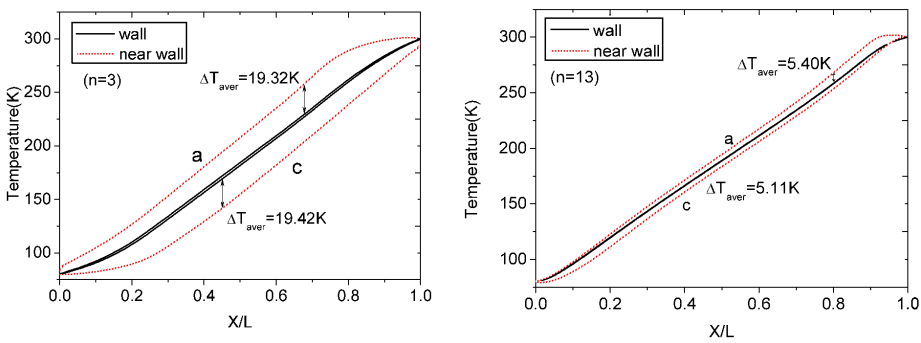

Figure 6. Temperature distribution near wall and on the wall at state a and c (non-adiabatic)

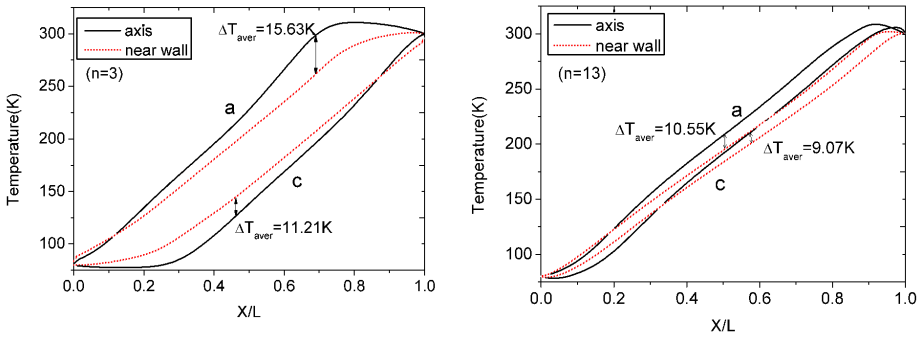

Figure 7. Temperature distribution near wall and on the axis at state a and c (non-adiabatic)

Figure 8 shows temperature distribution near wall and on the axis of pulse tube of 3 times the cold end expansion volume in the adiabatic model at state a and c. Figure 7 and 8 present that for pulse tube of the same volume (n=3), temperature difference between the gas near the wall and axis in the non-adiabatic model is larger than that in the adiabatic model, which is 4.67K in compression process and 0.93K in expansion process. The gas temperature on the same cross-section is more homogeneous in the adiabatic model than that in the non-adiabatic model. Hence, the heat exchange between the wall and the gas in the non-adiabatic model influences the gas temperature distribution on the cross-section and leads to a greater temperature difference between the gas near the wall and the main gas stream. In conclusion, the non-adiabatic wall not only brings in the shuttle loss but also increases the pumping loss near the wall.

Figure 9 shows the temperature difference between the wall and the gas near the wall. Figure 10 shows the temperature difference between the gas on axis and the gas near the wall. From these two figures, the two temperature differences in the non-adiabatic model is larger than that in the adiabatic model due to the exchange between the gas and the wall, which then causes a larger pumping loss and shuttle loss. With the increase in the pulse tube volume in the non-adiabatic model, the temperature difference decreases, and the non-adiabatic loss is reduced.

CONCLUSION

Based on the two-dimension non-adiabatic model, this paper presents the use of the CFD method to calculate an optimum pulse tube volume matching a constant cold end expansion volume. In the adiabatic model, when the pulse tube volume is 5-7 times the cold end expansion volume, the gas piston has the desirable ability for axial thermal insulation and gas flow insulation.

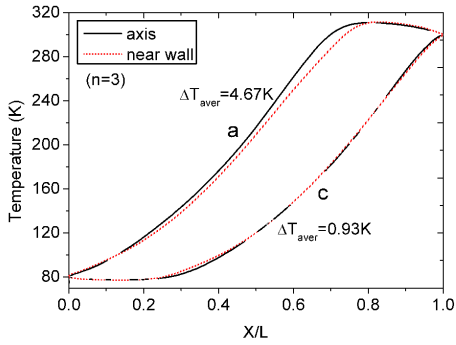

Figure 8. Temperature distribution near wall and on the axis at state a and c (adiabatic)

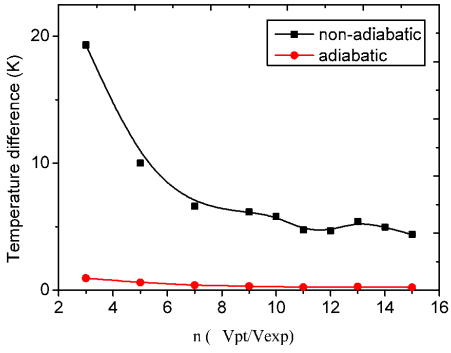

Figure 9. Temperature difference between wall and gas near wall of varied pulse tube volumes

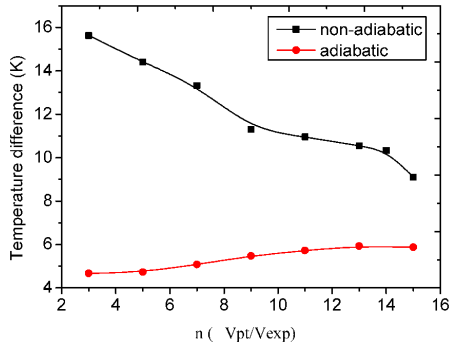

Figure 10. Temperature difference between gas on axis and gas near wall of varied pulse tube volumes

However, in the non-adiabatic model, a larger temperature difference between the gas near the wall and the wall and between the gas in the boundary layer and the main gas stream leads to a greater shuttle loss and pumping loss, thus optimum volume is 13 times the cold end expansion volume which is bigger than 5-7 times the cold end expansion volume obtained in the adiabatic model in order to reduce the influence of the non-adiabatic loss on expansion efficiency.

ACKNOWLEDGMENT

This work is financially supported by National Natural Science Foundation of China (No.51176165) and partially supported by the Open Project Program of the Key Laboratory of infrared imaging materials and detectors(IIMDKFJJ-11-07).

REFERENCES

1. Radebaugh, R., O'Gallagher, A., "Regenerator operation at very high frequencies for microcryocoolers," *Adv. in Cryogenic Engineering*, Vol. 51, Amer. Institute of Physics, Melville, NY (2006), pp. 1919-1928.
2. Vanapalli, S., Lewis M., Gan Z. H., Radebaugh, R., "120 Hz pulse tube cryocooler for fast cooldown to 50 K," *Applied Physics Letters,* Vol. 90, Issue 7 (February 2007), pp. 072504 – 072504-3.
3. Dai, W., Yu, G.Y., Zhu, S.L., et al, "300 Hz thermoacoustically driven pulse tube cooler for temperature below 100K," *Applied Physics Letters,* Vol. 90, Issue 2 (2007), pp. 024104 - 024104-3.
4. Zhu, S.L., Yu, G.Y., Dai, W., Luo, E.C., Wua, Z.H., Zhang, X.D., "Characterization of a 300 Hz thermoacoustically-driven pulse tube cooler," *Cryogenics,* Vol. 49, Issue 1 (January 2009), pp. 51–54.
5. Garaway, I., Gan, Z. H., Bradley, P., Radebaugh, R., "Development of a Miniature 150 Hz Pulse Tube Cryocooler," *Cryocoolers 15*, ICC Press, Boulder, CO (2009), pp. 105-113.
6. Petach, M., Waterman, M., Pruitt, G., Tward, E., "High Frequency Coaxial Pulse Tube Microcooler," *Cryocoolers 15*, ICC Press, Boulder, CO (2009), pp. 97-103.
7. Wu, Y.Z., Gan, Z.H., Qiu L.M., Chen J., Li, Z.P., "Study on a single-stage 120 Hz pulse tube cryocooler," *Adv. in Cryogenic Engineering*, Vol. 55, Amer. Institute of Physics, Melville, NY (2010), pp. 175-182.
8. Wang, X.T., Dai, W., Hu, J. Y., Luo, E. C., Zhou, Y., "Performance of a Stirling-type pulse tube cooler for high efficiency operation at 100Hz," *Cryocoolers 16*, ICC Press, Boulder, CO (2011), pp. 157-162.
9. Cai, H.K., Yang, L.W, Luo, E.C., Zhou, Y., "A 300 Hz two-stage pulse tube cryocooler that attains 58 K,", *Cryogenics, Vol. 50, Issue 8* (August 2010), pp. 469–471.

10. Lopes, D., Duval, J.-M., Charles I., Butterworth, J., Trollier, T., Tanchon, J., Ravex, A., Daniel, C., "Design and characterization of very high frequency pulse tube prototypes", *Adv. in Cryogenic Engineering*, Vol. 57, Amer. Institute of Physics, Melville, NY (2012), pp. 1487 – 1495.

11. Zhuopei, L., *Investigation on loss mechanism of high frequency regenerator at 4K and staging configuration of multi-stage pulse tube cryocooler*, Ph.D dissertation, (2010)

12. Cao, Q., *Investigation on the Refrigeration Mechanism of multi-stage Stirling Pulse Tube Cryocoolers working at Liquid-Helium Temperatures*, Phd dissertation (2012)

13. Zhi, X., Qiu, L., Gan, Z.H.,Yu, Y., Cao, Q., "Study of pulse tube losses based on a two-dimension non-adiabatic model," *Journal of Central South University*.

14. Yang, L.W., "Shuttle Loss in Pulse Tube," *Cryocoolers 11*, Kluwer Academic/Plenum Publishers, New York (2001), pp. 353-362.

15. Ming, W., Yaling, H., et. al., "Theoretical analysis and Numerical simulation of optimum ratio of pulse tube length to its diameter," *Xi'an Jiaotong University Journal*, Vol. 36, Issue 3 (2002), pp. 230-232.

16. Gedeon, D., *Sage Stirling-Cycle Model Class Reference Guide*, Athens, OH: Gedeon Associates, (2007).